Magnetic-Coupling Current-Balancing Cells Based Input-Parallel Output-Parallel *LLC* Resonant Converter Modules for High-Frequency Isolation of DC Distribution Systems

Chuang Liu, Xinzhe Xu, Dacheng He, Haiyang Liu, Xiaotong Tian, Ying Guo, Guowei Cai, Chenglian Ma, and Gang Mu

***Abstract*—The input-parallel output-parallel (IPOP) dc–dc converters are suitable for low-voltage and high-current applications, especially using high-frequency isolation instead of traditional line-frequency transformer for ac–dc converters in dc distribution. Compared to the existing closed-loop control for IPOP dc–dc converters, the magnetic-coupling current-balancing (MC-CB) cells based IPOP *LLC* resonant converter modules are proposed in this paper, which can realize the IPOP system work under open-loop operating condition naturally. The *LLC* modules can be used as a high-frequency isolation dc transformer operating under the quasi-resonant mode, which can achieve zero-voltage switching (ZVS) for inverter side and zero-current switching (ZCS) for rectifier side ensuring high power density and high efficiency. The proposed MC-CB cells for IPOP *LLC* resonant converter modules can adaptively ensure both the input-current sharing (ICS) and the output-current sharing (OCS) among constituent modules to make the IPOP system operate stably. Additionally, the steady-state and dynamic-state current-sharing performance of MC-CB cells for the IPOP converter system are analyzed based on a magnetic model. In the end, a hardware prototype has been designed and tested. The experimental results have verified the validity and performance of the proposed MC-CB cells for the IPOP *LLC* resonant converter modules.**

***Index Terms*—High-frequency isolation, input-parallel output-parallel (IPOP), *LLC* resonant converter, magnetic coupling current balancing (MC-CB) cell, quasi-resonant mode.**

Manuscript received June 14, 2015; revised September 9, 2015 and October 23, 2015; accepted November 29, 2015. Date of publication December 9, 2015; date of current version May 20, 2016. This work was supported by the National Natural Science Foundation of China under Grant 51307021 and Jilin Province Natural Science Foundation of China under Grant 20140101076JC. Recommended for publication by Associate Editor T. Qian.

C. Liu, D. He, H. Liu, X. Tian, Y. Guo, G. Cai, and G. Mu are with the Department of Electrical Engineering and Automation, Northeast Dianli University, Jilin 132012, China (e-mail: victorliuchuang@163.com; lyylhdc@163.com; lhy1122@126.com; 824653578@qq.com; 200828045@163.com; caigw@mail.nedu.edu.cn; mg@nedu.edu.cn).

X. Xu is with the Department of Electrical Engineering and Automation, Northeast Dianli University, Jilin 132012, China, and also with Beijing Electric Power Corporation, State Grid Corporation of China, Beijing 100031, China (e-mail: 1213278508@qq.com).

C. Ma was with the Department of Electrical Engineering and Automation, Northeast Dianli University, Jilin 132012, China. He is now with the School of Electrical and Electronic Engineering, North China Electric Power University, Beijing 102206, China (e-mail: machenglian@nedu.edu.cn).

Color versions of one or more of the figures in this paper are available online at http://ieeexplore.ieee.org.

Digital Object Identifier 10.1109/TPEL.2015.2507172

I. Introduction

RECENTLY, low-voltage dc distribution is the future trend for more efficient energy utilization, such as distributed renewable generation and less power conversion stages [1]–[6]. Compared to the traditional 50/60 Hz low-voltage ac distribution, there are no frequency stability and reactive power issues, as well as lower losses with less skin effect. Additionally, the consumer electronics, variable-speed motors, LED lighting, and electric vehicles (EVs) can be more conveniently powered by dc [7]–[10].

To construct dc distribution with galvanic isolation, the bidirectional ac–dc converter plays a key role and its basic function is to regulate the dc bus voltage and ac current based on the front-end line-frequency transformer or the back-end isolated dc converters [11]–[16]. To overcome the weight, size, and volume problems of line transformers, the isolated dc converters using high-frequency transformers are preferred, which can supply clean and stable power for dc distribution having high reliability, efficiency, effectiveness and maneuverability [15]–[29].

In order to increase the power rating of the isolated dc converters, the input-parallel output-parallel (IPOP) dc converter system can be used [30]–[33]. Fig. 1 shows a system infrastructure of a power control interface between low-voltage ac and dc distribution; the three-phase four-wire ac–dc converter can supply dc distribution with other functions such as three-phase power-imbalance regulation, reactive-power compensation, active-filtering, etc.; and the IPOP dc–dc converters can be widely used to provide dc voltage turn ratio, high-frequency isolation and high power rating.

The major advantage of the IPOP converter system is that the current stresses on the power devices of the constituent modules can be reduced. The IPOP dc–dc converter modules have been the subject of vigorous research recently, which is used in many applications requiring low voltage and high current, and it is conducive to the systems' expansion and redundancy. For the traditional IPOP dc–dc converter modules, the basic objectives that guarantee the stable operation are to ensure input-current sharing (ICS) and output-current sharing (OCS) among the constituent modular converters. The control strategies aiming to achieve ICS and OCS for the IPOP converter system have been studied extensively, however, the existing control strategies for IPOP converter systems are complicated having poor

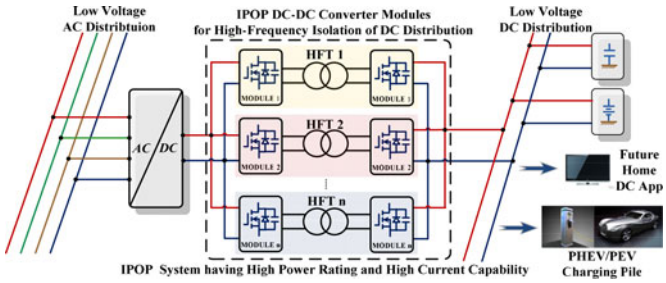

Fig. 1. AC–DC converters based on IPOP dc–dc converters for low-voltage ac and dc distribution.

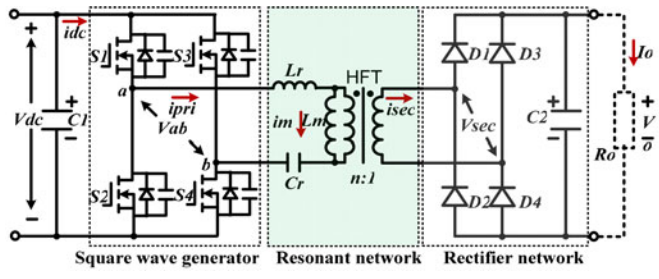

Fig. 2. Schematic of the full-bridge *LLC* resonant converter.

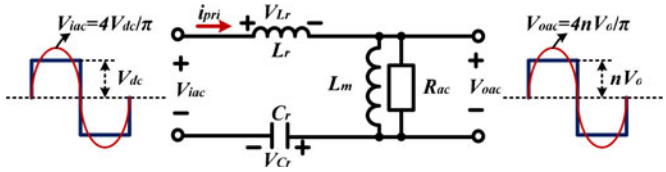

Fig. 3. AC equivalent circuit for full-bridge *LLC* resonant converter.

reliability, and the cost of the sensing circuit components for the closed-loop operation is high.

Among the dc–dc converters [15]–[29], the *LLC* resonant converter has superior performance compared to the others, such as zero-voltage and zero-current switching (ZVZCS) [22]–[29]. In order to fully utilize the potential of the *LLC* resonant converter, the IPOP *LLC* resonant converter modules are adopted. Because the *LLC* resonant converter modules can be used as high-frequency isolation dc transformers operating under the quasi-resonant mode, the magnetic-coupling current-balancing (MC-CB) cells for the IPOP *LLC* resonant converter modules are proposed to solve the current balancing problem. The IPOP *LLC* resonant converter modules employ the proposed MC-CB cells to achieve ICS and OCS among the constituent modules, so the each module can work under open-loop operation condition. Thus, the proposed whole IPOP converter system has the advantages of high reliability, easy expansion, low cost, etc.

This paper is organized as follows. The features and characteristics of *LLC* resonant converter and the IPOP converter system based on *LLC* resonant converter modules are introduced in Section II. Section III addresses the electric model of the MC-CB-cell-based IPOP converter system and the current-sharing performance of MC-CB cells for the IPOP *LLC* resonant converter modules are analyzed based on the magnetic model. In Section IV, in order to verify the validity and performance of the proposed MC-CB cells for IPOP system, a hardware prototype has been designed, fabricated and tested and the experimental results has showed the good performance of the MC-CB cells for the IPOP system. Finally, the conclusion is drawn in Section V.

II. IPOP System Based on *LLC* Resonant Converter Modules

A. Features and Characteristics of LLC Resonant Converter

The basic function of the *LLC* resonant converter operating under the quasi-resonant mode is just like a high-frequency isolation dc transformer, which can achieve zero-voltage switching (ZVS) for the inverter side and zero-current switching (ZCS) for the rectifier side ensuring high efficiency and high power density. In this paper, *LLC* resonant converter is adopted for the proposed IPOP system and the simplified schematic of the full-bridge *LLC* resonant converter is shown in Fig. 2, where L_m is the magnetizing inductance that acts as a shunt inductor, L_r is the series leakage inductance that acts as the series resonant inductor, and C_r is the resonant capacitor. In general, the *LLC* resonant converter topology consists of three stages: the square wave generator, resonant network and rectifier network.

Comparing with the other dc–dc converter, *LLC* resonant converter has the following advantages:

1) ZVS capability from zero- to full-load range, low MOSFET turn-off current, so the switching loss is very low;
2) low voltage stress on secondary rectifier; because for this converter, there is no secondary filtering inductor;
3) the magnetic components can be easily integrated into one magnetic core and the leakage inductance of the transformer can be utilized;
4) when *LLC* resonant converter operates at the quasi-resonant frequency, the voltage gain is almost constant and independent of the load;
5) the series resonant capacitor C_r provides dc blocking favorable for isolation transformer.

For the purposed model of the full-bridge *LLC* resonant converter, the ac equivalent electrical circuit as shown in Fig. 3 has been considered.

So the output dc load R_o is replaced by the ac equivalent load $R_{\rm ac}$ and expressed as follows, where *n* is the transformer turns ratio:

$$R_{\rm ac} = \frac{8n^2 R_o}{\pi^2}. \tag{1}$$

The *LLC* resonant converter switching frequency f_s can be operated above, at or below the resonant frequency f_r shown as follows:

$$f_r = \frac{1}{2\pi\sqrt{L_r C_r}}. \tag{2}$$

Using the ac equivalent circuit of Fig. 3, the *LLC* resonant converter ac equivalent input voltage and output voltage are

shown as follows:

$$V_{\text{inac}} = \frac{4V_{\text{dc}}}{\pi}\sin\omega t \tag{3}$$

$$V_{\text{oac}} = \frac{4nV_o}{\pi}\sin\omega t. \tag{4}$$

And the ac equivalent current can be obtained as

$$I_{\text{pri}} = \frac{(4nV_o/\pi)\sin\omega t}{X_{L_m}//R_{\text{ac}}}. \tag{5}$$

So the *LLC* resonant converter voltage gain *M* is obtained as

$$M = \frac{1}{\sqrt{\left[\frac{L_r}{L_m}\left(\frac{\omega_s^2}{\omega_s^2}-1\right)\frac{\omega_r^2}{\omega_r^2}\right]^2 + \left[\frac{\pi^2}{8}Q\left(\frac{\omega_s}{\omega_r}-\frac{\omega_r}{\omega_s}\right)\right]^2}} \tag{6}$$

Here

$$\omega_r = \frac{1}{\sqrt{L_rC_r}}, \qquad \omega_m = \frac{1}{\sqrt{(L_r+L_m)C_r}},$$

$$Q = \frac{1}{n^2R_o}\sqrt{\frac{L_r}{C_r}}.$$

Assuming $\alpha = L_m/L_r$ and $\gamma = f_s/f_r$, (7) can be derived

$$M = \frac{1}{\sqrt{((1/\alpha)+1-(1/\alpha\gamma^2))^2 + (\pi^4/64)Q^2((1/\gamma)-\gamma)^2}}. \tag{7}$$

Magnetizing inductance L_m selection is a trade-off between the minimum dead time limitation for ZVS under no load condition and the current stress of MOSFETs. Since the magnetizing inductor L_m is relatively small, there exists considerable amount of magnetizing current i_m, which freewheels in the primary side without being involved in the power transfer. The primary-side current i_{pri} is the sum of the magnetizing current i_m and the secondary-side current i_{sec} referred to the primary. Due to the *LLC* resonant converter operating at the high quasi-resonant frequency, the converter can achieve ZVS for the inverter side and ZCS for the rectifier side ensuring high power density with isolation and high efficiency.

According to the related papers [22]–[29], an *LLC* resonant converter with 60 kHz resonant frequency has been designed where the key parameters are $L_r = 8.24$ μH, $L_m = 83.8$ μH, and $C_r = 1$ μH. Using the frequency response analyzer (VENABLE Model 3120) where $V_{i\text{ac}} = \pm 1$ V and $R_o = (1.6\ \Omega, 3.2\ \Omega, 6.4\ \Omega, 16\ \Omega, 40\ \Omega, 160\ \Omega)$, the experimental voltage gain characteristics of the *LLC* resonant converter is shown in Fig. 4. As observed in Fig. 4, the *LLC* resonant converter shows the voltage gain characteristics, which are almost independent of the load when the switching frequency f_s is around the resonant frequency f_r, so the *LLC* resonant converter is just like a high-frequency isolation dc transformer operating under the quasi-resonant mode. This is a distinct advantage of *LLC* resonant converter compared to the other dc–dc converters, which is a good application for IPOP converter system.

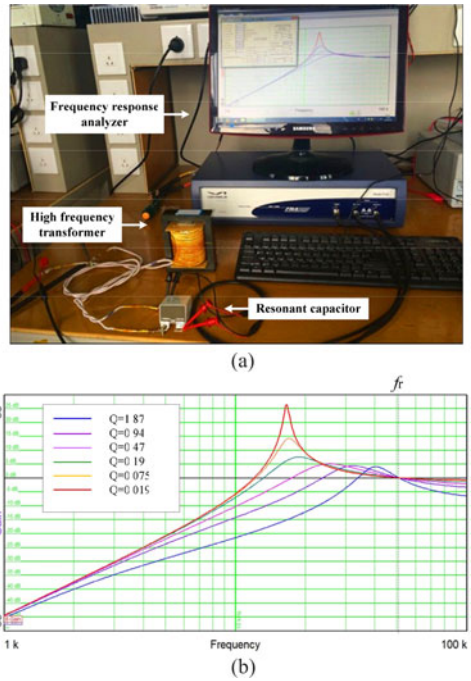

Fig. 4. Voltage gain characteristics of *LLC* resonant converter: (a) Frequency response analyzer (VENABLE Model 3120) and (b) voltage gain characteristics.

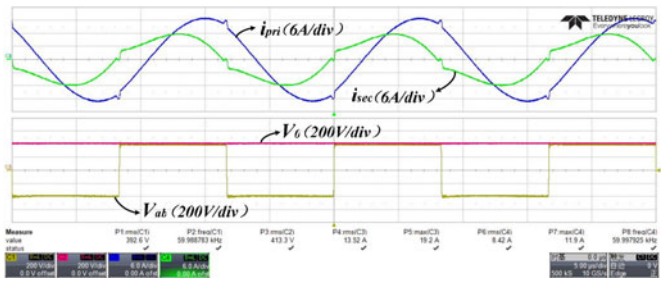

Fig. 5. Experimental waveforms of the *LLC* resonant converter.

Fig. 5 shows the experimental waveforms at the 3-kW power level, with $f_s = 60$ kHz switching frequency, including the waveforms of the primary-side current i_{pri}, the secondary-side current i_{sec}, the primary-side voltage V_{ab}, and the output voltage V_o. The transformer turns ratio is about $n = 1{:}1$, and the input voltage $V_{\text{dc}} = 400$ V and the output voltage $V_o = 400$ V. The experimental results verify the good performance of *LLC* resonant converter, so it can be used as a standardized module in the IPOP converter system.

B. IPOP Converter System Based on LLC Resonant Converter Modules

LLC resonant topology has been widely adopted; however, when the current level increases, the *LLC* topology has the following limitations:

1) the secondary-side conduction loss is high, which decreases the heavy-load efficiency;
2) the output current ripple is high, which requires large output capacitance;

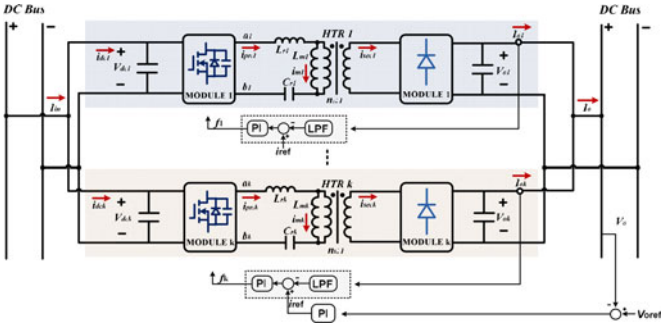

Fig. 6. Master–slave control scheme for IPOP *LLC* resonant converter modules.

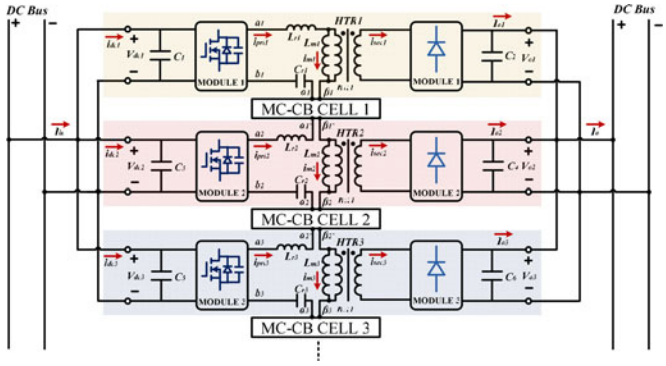

Fig. 7. Proposed MC-CB cells for multimodule IPOP *LLC* resonant dc–dc converter system.

3) the primary-side component stress is high, which limits the maximum power capacity;
4) the circulation current is high, which decreases the light-load efficiency.

The aforementioned problems can be solved by using the IPOP *LLC* resonant converter modules as proposed in this paper. With the multimodule IPOP topology [30]–[33], the high conduction loss can be reduced by splitting current into multiple modules; the high current ripple can be cancelled by multiple modules; the power capacity can be easily expanded without the increasing component stress; and the light-load efficiency can be improved by module shedding. The IPOP *LLC* resonant converter modules can separately experience the lower input current so that the lower current rating device MOSFETs and diodes can be used to ensure the high reliability and high power density with higher switching frequency operation.

In steady-state operation of the IPOP converter system, the difference in the transformer turn ratios and module parameter mismatches will result in power imbalance and unequal current sharing among the constituent modules, which will make the IPOP converter system unreliable. For the IPOP converter system, the objective to transmit power evenly can be realized by ensuring ICS and OCS among the constituent modules. One existing method of the master–slave control scheme [34] is presented for IPOP *LLC* resonant converter modules, as shown in Fig. 6.

The control loops include a master voltage loop and a master–slave load sharing loop that aims to maintain the output voltage at the desired reference voltage and achieve the load current sharing. The output voltage signal V_o is sampled by the master manipulator and then subtract the reference voltage $V_{\rm ref}$ to create a voltage error value. The voltage error value is processed by a PI controller to generate the desired reference current $I_{\rm ref}$. The load current signals $I_{\rm ok}(k = 1, 2, \ldots)$ are sampled by the master–slave manipulator and then subtract the reference current $I_{\rm ref}$ to create a current error processed by a load-sharing controller to generate the variable control switching frequencies $f_k(k = 1, 2, \ldots)$ for the constituent modules. However the different variable frequencies' control to make the output current balancing between the constituent *LLC* modules is difficult to realize in practical applications.

III. Proposed MC-CB Cells For IPOP *LLC* Modules

In this paper the MC-CB cells are proposed for the adopted IPOP *LLC* resonant converter modules to achieve the ICS and OCS of the constituent modules under the open-loop operation condition as shown in Fig. 7. The MC-CB cell is connected between the leading-leg midpoint of one module and the lagging-leg midpoint of the other one. In this way, the primary-side current of two modules, such as $i_{\rm pri1}$ and $i_{\rm pri2}$, can be regulated nearly the same by the magnetic coupling of the MC-CB cells. One MC-CB cell can balance two *LLC* modules current evenly; thus, an n-module IPOP converter system needs $(n - 1)$ MC-CB cells.

Compared with the existing IPOP converter system, which employs the control strategies [30]–[35], to achieve ICS and OCS, the proposed MC-CB-cell-based IPOP *LLC* resonant converter modules have the following characteristics:

1) through the magnetic coupling of the proposed MC-CB cells, the IPOP *LLC* converters' system can work under the quasi-resonant mode without the variable frequency control and other control strategies having the dc transformer function;
2) the auxiliary sampling and control circuits can be avoided; thus, the number of components can be decreased significantly to reduce the cost;
3) without the complicated multiloop control scheme to achieve ICS and OCS, the whole IPOP converter system has higher reliability.

However, comparing the traditional control strategies, the main disadvantage of the proposed MC-CB cells is that the magnetic element may be increased to decrease the power density a little.

A. Steady-State Electrical Model and Current-Sharing Performance

1) IPOP LLC System Electrical Model: As shown in Fig. 7, the *LLC* resonant converter modules are coupled together by the MC-CB cells with galvanic isolation, for the MC-CB cell 1, the primary-side current $i_{\rm pri1}$ of the *LLC* resonant converter module 1 flowing through the MC-CB cell 1 generates the large magnetic flux B_{11} pointing to one direction in the common

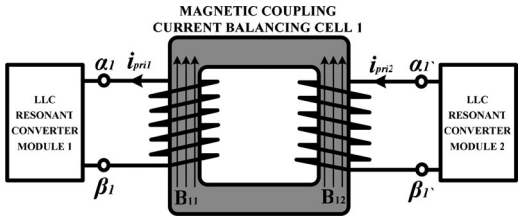

Fig. 8. Magnetic model of MC-CB cell 1 for IPOP system.

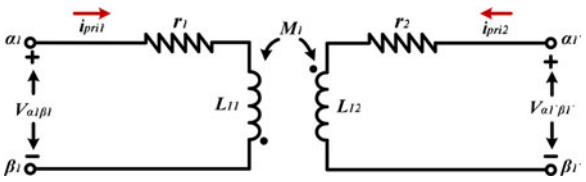

Fig. 9. Electrical model of the proposed MC-CB cell.

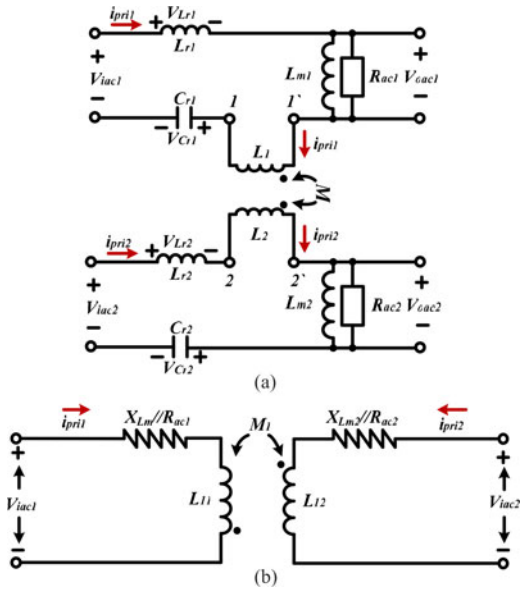

Fig. 10. AC equivalent model of proposed MC-CB cell based two-module IPOP *LLC* resonant converter system. (a) Detailed ac equivalent model. (b) Simplified ac equivalent model.

magnetic core and the *LLC* resonant converter module 2 primary-side current i_{pri2} generates the opposite magnetic flux B_{12} versus the B_{11} in the same way. Since the primary-side current i_{pri1} and i_{pri2} of each module are nearly the same, the effective magnetic flux in the MC-CB cell 1 core can be cancelled; in this way, the imbalance current can be limited. The detailed magnetic model of the proposed MC-CB cell 1 for IPOP system is shown in Fig. 8.

Based on the MC-CB cell 1 magnetic model, the corresponding electrical model can be built as shown in Fig. 9.

The induced voltages of the MC-CB cell 1 are shown as follows:

$$\begin{cases} V_{\alpha 1\beta 1} = \dfrac{d\psi_{11}}{dt} + i_{\mathrm{pri1}} r_1 \\ V_{\alpha 1'\beta 1'} = \dfrac{d\psi_{12}}{dt} + i_{\mathrm{pri2}} r_2 \end{cases}. \tag{8}$$

The MC-CB cell 1 equivalent resistance r_1 and r_2 is relatively small that can be ignored, so the MC-CB-cell-1 induced voltage can be written as follows:

$$\begin{cases} V_{\alpha 1\beta 1} = V_{L_{11}} = L_{11}\dfrac{di_{\mathrm{pri1}}}{dt} - M_1\dfrac{di_{\mathrm{pri2}}}{dt} \\ V_{\alpha 1'\beta 1'} = V_{L_{12}} = L_{12}\dfrac{di_{\mathrm{pri2}}}{dt} - M_1\dfrac{di_{\mathrm{pri1}}}{dt} \end{cases} \tag{9}$$

where L_{11} and L_{12} are the self-inductances of the MC-CB cell 1, respectively, M_1 is the mutual inductance of the MC-CB cell 1. For the strong coupling of the MC-CB cell, the self-inductances L_{11} and L_{12} and the mutual inductance M_1 are nearly the same. Thus, we can assume that $L_{11} = L_{12} = M_1$.

When the proposed IPOP converter system working around the resonant frequency f_r and the secondary-side resistance R_0 referred to the primary side, we can get the ac equivalent circuit of the proposed two-module IPOP *LLC* resonant converter system, with one MC-CB cell as shown in Fig. 10(a). The effect of the leakage inductance L_r and the resonant capacitor C_r can be offset because of $j\omega_r L_r + 1/j\omega_r C_r = 0$. Thus, the simplified electrical model of the proposed IPOP system can be built as shown in Fig. 10(b).

From the electrical model in Fig. 10, it can be seen that

$$\begin{cases} V_{\mathrm{iac1}} = (X_{Lm1}//R_{\mathrm{ac1}})i_{\mathrm{pri1}} + V_{L_{11}} \\ V_{\mathrm{iac2}} = (X_{Lm2}//R_{\mathrm{ac2}})i_{\mathrm{pri2}} + V_{L_{12}}. \end{cases} \tag{10}$$

Also we can get the ac equivalent circuit of the proposed k-module IPOP *LLC* resonant converter system with (k – 1) MC-CB cells, as shown in Fig. 11.

From the electrical model of Fig. 11, there are

$$\begin{cases} V_{\mathrm{iac1}} = (X_{Lm1}//R_{\mathrm{ac1}})i_{\mathrm{pri1}} + V_{L_{11}} \\ V_{\mathrm{iac2}} = (X_{Lm2}//R_{\mathrm{ac2}})i_{\mathrm{pri2}} + V_{L_{12}} + V_{L_{21}} \\ V_{\mathrm{iac3}} = (X_{Lm2}//R_{\mathrm{ac2}})i_{\mathrm{pri2}} + V_{L_{22}} + V_{L_{31}} \\ \vdots \\ V_{\mathrm{iac}(k-1)} = (X_{Lm(k-1)}//R_{\mathrm{ac}(k-1)})i_{\mathrm{pri}(k-1)} + V_{L_{(k-2)2}} \\ \qquad\qquad + V_{L_{(k-1)1}} \\ V_{\mathrm{iac}k} = (X_{Lmk}//R_{\mathrm{ack}})i_{\mathrm{pri}k} + V_{L_{(k-1)2}}. \end{cases} \tag{11}$$

2) Steady-State Current-Sharing Performance: First, the steady-state current-sharing performance of MC-CB cell can be analyzed. Under the condition of $i_{\mathrm{pri1}} = i_{\mathrm{pri2}}$, the ICS and OCS among the constituent modules can be achieved from (9). We can get the MC-CB-cell-1 induced voltages $V_{L11} = V_{L12} = 0$. In a similar way, all the MC-CB-cell-induced voltages $V_{L11} = V_{L12} = V_{L21} = V_{L22} = \ldots = V_{L(k-1)1} = V_{L(k-2)2} = 0$. So the electrical model of Fig. 11

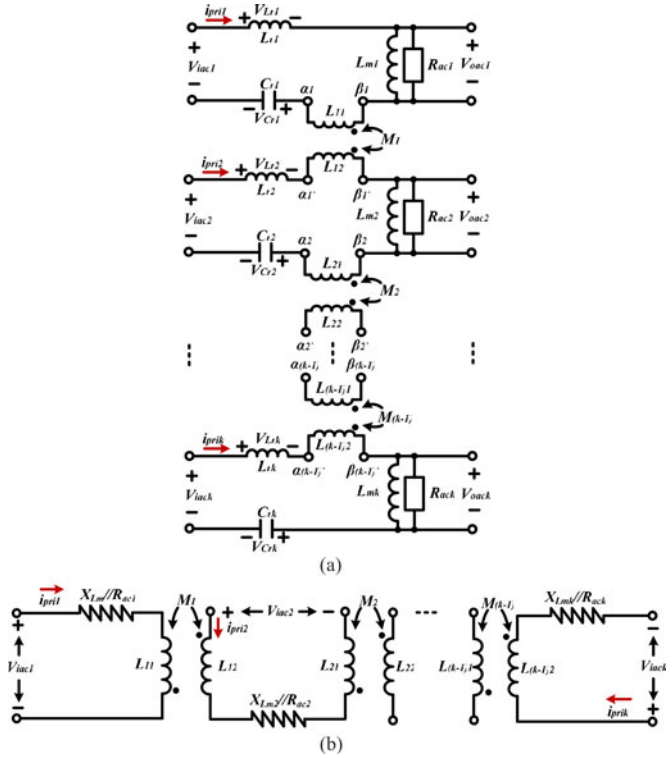

Fig. 11. AC equivalent model of the proposed MC-CB cells based *k*-module IPOP *LLC* resonant converter system. (a) The detailed ac equivalent model. (b) The simplified ac equivalent model.

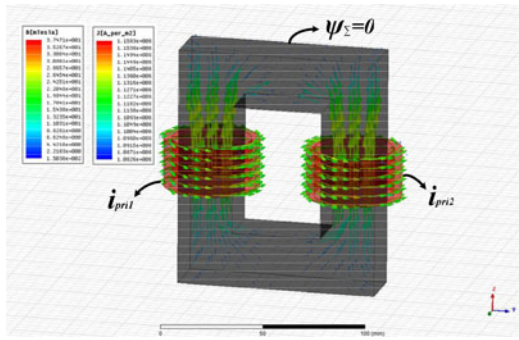

Fig. 12. Simulation of MC-CB cells' magnetic model on the occasion $i_{\mathrm{pri1}} = i_{\mathrm{pri2}}$.

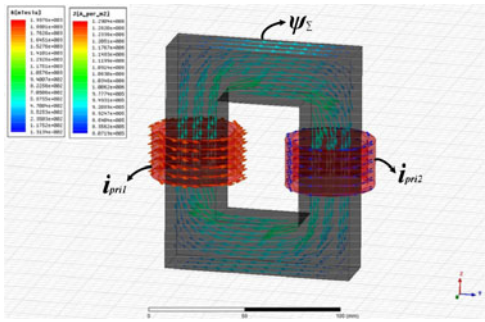

Fig. 13. Simulation of CB's magnetic model on the occasion $i_{\mathrm{pri1}} \geq i_{\mathrm{pri2}}$.

can be written as follows:

$$\begin{cases} V_{iac1} = (X_{Lm1}//R_{\mathrm{ac1}})i_{\mathrm{pri1}} = \dfrac{4n_1V_o}{\pi}\sin\omega t \\ V_{\mathrm{iac2}} = (X_{Lm2}//R_{\mathrm{ac2}})i_{\mathrm{pri2}} = \dfrac{4n_2V_o}{\pi}\sin\omega t \\ V_{\mathrm{iac3}} = (X_{Lm2}//R_{\mathrm{ac2}})i_{\mathrm{pri2}} = \dfrac{4n_3V_o}{\pi}\sin\omega t \\ \vdots \\ V_{\mathrm{iac}(k-1)} = (X_{Lm(k-1)}//R_{\mathrm{ac}(k-1)})i_{\mathrm{pri}(k-1)} \\ \qquad\qquad = \dfrac{4n_{(k-1)}V_o}{\pi}\sin\omega t \\ V_{\mathrm{iack}} = (X_{Lmk}//R_{\mathrm{ack}})i_{\mathrm{prik}} = \dfrac{4n_kV_o}{\pi}\sin\omega t. \end{cases} \tag{12}$$

All the ac equivalent input voltages are only affected by the transformer turns ratio, which have a small mismatch, and they are nearly the same. The simulation results of MC-CB cell 1 magnetic model on the occasion that $i_{\mathrm{pri1}} = i_{\mathrm{pri2}}$ is shown in Fig. 12 where the MC-CB cell's magnetic flux $\psi = 0$.

B. Dynamic-State Current-Sharing Performance of MC-CB Cell

Next, we focus on the dynamic-state current-sharing performance of MC-CB cell 1. On the occasion that $i_{\mathrm{pri1}} \neq i_{\mathrm{pri2}}$, assuming that $i_{\mathrm{pri1}} \geq i_{\mathrm{pri2}}$, according to the Ampere circuital theorem, the total MC-CB cell 1 magnetic flux ψ is given as follows:

$$\psi = \frac{\mu_i N_{\mathrm{CB}}\left(i_{\mathrm{pri1}} - i_{\mathrm{pri2}}\right)S}{L_R} \tag{13}$$

where μ_i is the permeability, N_{CB} is the turns of winding, S is the cross-sectional area of magnetic core, and L_R is the mean length of magnetic circuit.

According to the Lenz's law, the MC-CB cell 1 magnetic flux ψ generates the induced electromotive force that the MC-CB-cell-1 induced voltages V_{L11} will decrease and V_{L12} will increase until $V_{L11} = V_{L12} = 0$. In a similar way, the MC-CB cell 1 current i_{pri1} will decrease and i_{pri2} will increase until $i_{\mathrm{pri1}} = i_{\mathrm{pri2}}$. The other MC-CB cells have the same function of current balance between each other. The simulation of MC-CB cell's magnetic model on the occasion that $i_{\mathrm{pri1}} \geq i_{\mathrm{pri2}}$ is shown in Fig. 13, where the MC-CB cell's magnetic flux $\psi > 0$.

C. MC-CB Selector for Adding and Returning Modules Under the Load Condition

In order to prove the MC-CB cells can work well when the modules currents have a big difference initially, the MC-CB selectors are designed and fabricated. The MC-CB selector is adopted for adding and returning modules on load, and the electrical model can be built, as shown in Fig. 14.

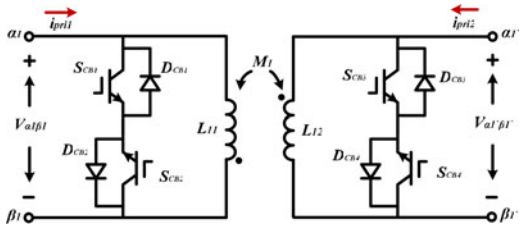

Fig. 14. Electrical model of MC-CB selector.

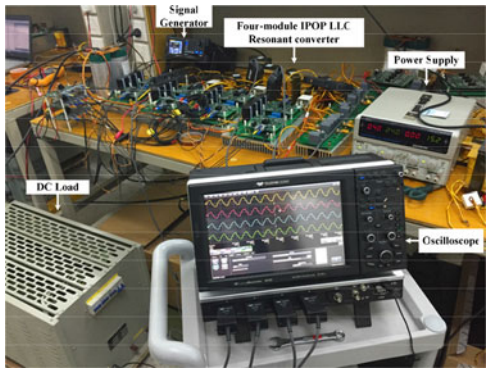

Fig. 15. Four-module IPOP system experimental setup.

TABLE I
CIRCUIT PARAMETERS OF IPOP *LLC* RESONANT CONVERTER SYSTEM

Designation	Parameters
Input voltage $V_{\rm dc}$	100 V
Output voltage V_o	100 V
Transformer turns ratio n	1:1
MC-CB cell turns of winding $N_{\rm CB}$	6
Switching frequency f_s	60 kHz

The MC-CB selector can realize adding and returning modules under the load condition easily. When the module 1 is working and module 2 is shut off, the switches ($S_{\rm CB1}, S_{\rm CB2}, S_{\rm CB3}, S_{\rm CB4}$) should be kept on to short the primary and secondary sides of the MC-CB cell. Thus, there is no additional inductance to module 1. When the both module 1 and module 2 are working, the switches ($S_{\rm CB1}, S_{\rm CB2}, S_{\rm CB3}, S_{\rm CB4}$) are kept off and the MC-CB cell can enter the circuit that achieve ICS and OCS naturally.

IV. EXPERIMENTAL RESULTS

In order to verify viability and merits of the proposed MC-CB-cell-based IPOP *LLC* resonant converter modules, a four-module IPOP *LLC* system prototype has been designed, fabricated, and tested. The photograph of the hardware prototype is shown in Fig. 15, the specifications of the prototype are shown in Table I, and the devices and components of the prototype are shown in Table II.

TABLE II
DEVICES AND COMPONENTS OF IPOP *LLC* RESONANT CONVERTER SYSTEM

Device	Type
LLC switching devices S_1–S_{16}	IPW65R041CFD
LLC rectifier diodes D_1–D_{16}	IDW40G65C5
LLC resonant capacitor $C_{r1}, C_{r2}, C_{r3}, C_{r4}$	C4BSNBX4100ZAFJ
Regulated capacitor C_1–C_8	UP3-21484K
Transformer core	E80/38/20-3C95
MC-CB cells core	E100/60/28-3c94

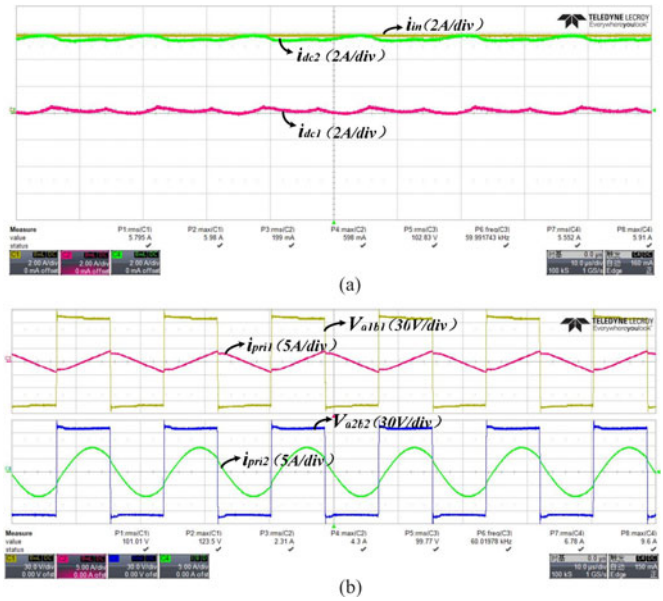

Fig. 16. Experimental results of two-module IPOP system without the MC-CB cell: (a) Total input current $i_{\rm in}$ and the two-module input current ($i_{\rm dc1}, i_{\rm dc2}$). (b) Primary-side voltages ($V_{\rm a1b1}, V_{\rm a2b2}$) and currents ($i_{\rm pri1}, i_{\rm pri2}$).

A. Two-Module IPOP LLC Resonant Converter System Performance

When the two-module IPOP *LLC* resonant converter system works under the open-loop operation, it is necessary to analyze the steady-state current-sharing performance without the MC-CB cell. When the input dc voltage is 100 V and the resistive load $R_0 = 20\ \Omega$, Fig. 16(a) shows the total input current $i_{\rm in}$ and the two-module input currents ($i_{\rm dc1}, i_{\rm dc2}$) without the MC-CB cell and Fig. 16(b) shows the primary-side voltages ($V_{\rm a1b1}, V_{\rm a2b2}$) and currents ($i_{\rm pri1}, i_{\rm pri2}$). The transformer turn ratios and module parameter only have small mismatches, namely, $n_1 = 1.03$, $n_2 = 0.99$, $L_{r1} = 7.99\ \mu$H, $L_{r2} = 8.24\ \mu$H, $L_{m1} = 90.3\ \mu$H, and $L_{m2} = 83.8\ \mu$H. From Fig. 16, we can see that the one-module input current of the IPOP system $i_{\rm dc1}$ is almost zero and $i_{\rm dc2}$ is almost equal to $i_{\rm in}$. Additionally, there is a big difference between the primary-side currents ($i_{\rm pri1}, i_{\rm pri2}$) of the two *LLC* resonant converters. Thus, it is confirmed that the total input current $i_{\rm in}$ has been shared unevenly between the two modules even though the mismatch is relatively small.

1) Steady-State Operation: The proposed MC-CB cell is adopted to solve the current unbalance between the two *LLC* resonant converter modules working under the quasi-resonant

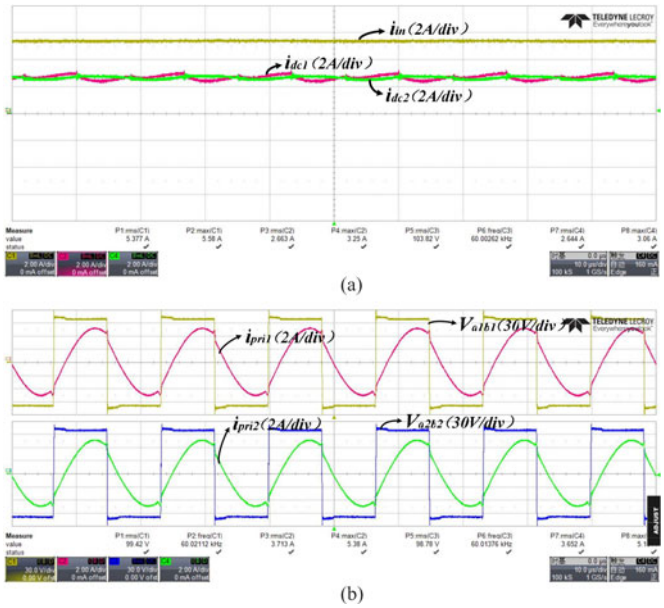

Fig. 17. Experimental results of two-module IPOP system with the MC-CB cell: (a) Total input current $i_{\rm in}$ and the two-module input currents ($i_{\rm dc1}, i_{\rm dc2}$). (b) Primary-side voltages ($V_{\rm a1b1}, V_{\rm a2b2}$) and currents ($i_{\rm pri1}, i_{\rm pri2}$) of two *LLC* resonant converters.

mode. When the input voltage is 100 Vdc and the resistive load $R_0 = 20\ \Omega$, Fig. 17(a) shows the total input current $i_{\rm in}$ and the two-module input currents ($i_{\rm dc1}, i_{\rm dc2}$) with the MC-CB cell. Fig. 17(b) shows primary-side voltages ($V_{\rm a1b1}, V_{\rm a2b2}$) and currents ($i_{\rm pri1}, i_{\rm pri2}$). In Fig. 17(a), the input currents ($i_{\rm dc1}, i_{\rm dc2}$) of the two modules are maintained nearly constant sharing equally, which has verified the good performance of the MC-CB cell in the steady-state operation. From Fig. 17(b), the primary-side currents ($i_{\rm pri1}, i_{\rm pri2}$) of the two *LLC* resonant converters are also nearly the same. Therefore, it is experimentally verified that the MC-CB cell can realize the ICS and OCS of the two-module IPOP converter system in the steady-state operation in the presence of mismatched module parameters.

2) Dynamic-State Operation: In order to verify the MC-CB effectiveness in the dynamic-state operation, a load step is made to see the two-module IPOP *LLC* resonant converter system may undertake higher current exceeding the current ratings of switching devices. Hence, it is necessary to analyze the dynamic-state current-sharing performance of the two-module IPOP converter system. Fig. 18(a) and (b) gives the transient waveforms of two *LLC* resonant converters secondary-side voltages ($V_{\rm sec1}, V_{\rm sec2}$) and currents ($i_{\rm sec1}, i_{\rm sec2}$) during a step up and a step down of resistive load between $R_0 = 16$ and $27\ \Omega$. As seen from Fig. 18, both the two currents ($i_{\rm sec1}, i_{\rm sec2}$) shows the same change trend when the resistive load transients and quickly achieve a new balance, the output voltages ($V_{\rm sec1}, V_{\rm sec2}$) are unaffected during the load transients.

B. Three-Module and Four-Module IPOP LLC Resonant Converter System Performance

In order to verify that the MC-CB cells can be employed to the multimodule IPOP *LLC* resonant converter system, a

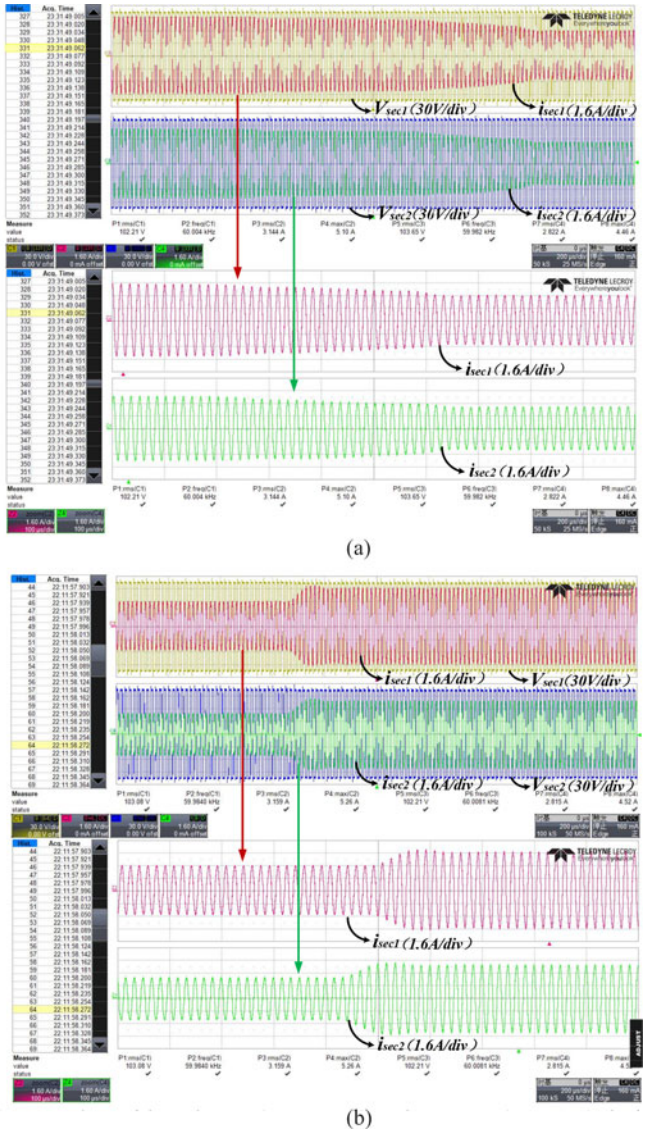

Fig. 18. Transient waveforms of two *LLC* resonant converters. (a) Secondary-side voltages ($V_{\rm sec1}, V_{\rm sec2}$) and currents ($i_{\rm sec1}, i_{\rm sec2}$) during a step up of resistive load from $R_0 = 16\ \Omega$ to $R_0 = 27\ \Omega$. (b) Secondary-side voltages ($V_{\rm sec1}, V_{\rm sec2}$) and currents ($i_{\rm sec1}, i_{\rm sec2}$) during a step down of resistive load from $R_0 = 27\ \Omega$ to $R_0 = 16\ \Omega$.

three-module IPOP converter system prototype consisting of three *LLC* resonant converter modules and two MC-CB cells is constructed and tested. When the input voltage is 100 Vdc and the resistive load $R_0 = 16\ \Omega$, Fig. 19(a) shows the input voltage $V_{\rm in}$ and the three-module input currents ($i_{\rm dc1}, i_{\rm dc2}, i_{\rm dc3}$) with MC-CB cells. Fig. 19(b) shows primary-side voltage V_{a1b1} and currents ($i_{\rm pri1}, i_{\rm pri2}, i_{\rm pri3}$) of three *LLC* resonant converter modules with MC-CB cells. In Fig. 19(a), the waveforms of input currents ($i_{\rm dc1}, i_{\rm dc2}, i_{\rm dc3}$) are nearly overlap, so the input currents of three modules are shared equally. From Fig. 19(b), the primary-side currents ($i_{\rm pri1}, i_{\rm pri2}, i_{\rm pri3}$) of the three *LLC* resonant converters are controlled having the same values. Thus, it is verified that the MC-CBs can be employed for the three-module IPOP *LLC* resonant converter system to achieve ICS and OCS in the steady-state operation.

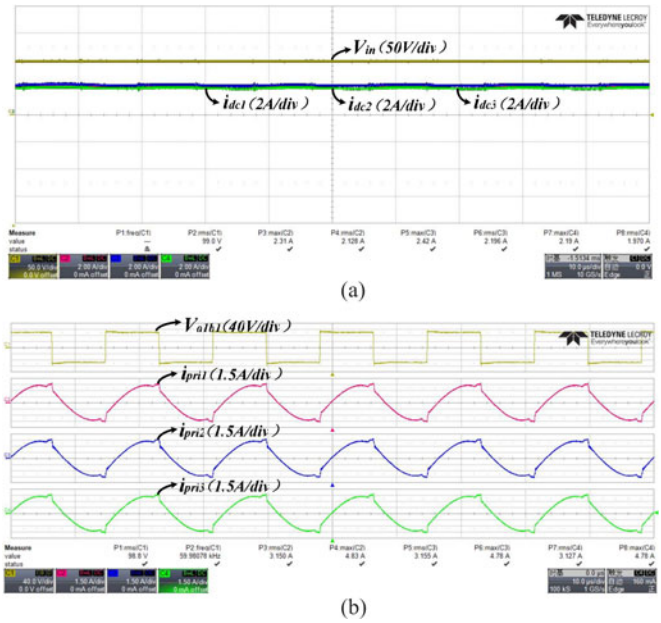

Fig. 19. Experimental results of three-module IPOP system with two MC-CB cells: (a) Input voltage $V_{\rm in}$ and the three-module input currents $(i_{\rm dc1}, i_{\rm dc2}, i_{\rm dc3})$. (b) Primary-side voltage $V_{\rm a1b1}$ and currents $(i_{\rm pri1}, i_{\rm pri2}, i_{\rm pri3})$ of three *LLC* resonant converter modules.

Fig. 20(a) and (b) gives the transient waveforms of three *LLC* resonant converter modules secondary-side voltage $V_{\rm sec1}$ and currents $(i_{\rm sec1}, i_{\rm sec2}, i_{\rm sec3})$ during a step up and a step down of resistive load between $R_0 = 16$ and 27 Ω. From Fig. 20, we can see all the currents $(i_{\rm sec1}, i_{\rm sec2}, i_{\rm sec3})$ have the same change trend and achieve a new balance at the same time and the output voltages $V_{\rm sec1}$ are unaffected during the load transients.

Also, a four-module IPOP converter system prototype consisting of four *LLC* resonant converter modules and three MC-CB cells is constructed and tested when the input voltage is 100 Vdc and the resistive load $R_0 = 8$ Ω. Fig. 21 shows the steady-state and dynamic-state current-sharing performance of the IPOP converter system, which verify the good ability of MC-CB cells.

C. MC-CB Selector for Adding and Returning Modules Under the Load Condition

The proposed MC-CB selector is adopted to solve the problem of adding and returning modules on load when the two *LLC* resonant converter modules working under the quasi-resonant mode. The system parameters are as follows: the input voltage $V_{\rm dc} = 100$ Vdc and the resistive load $R_0 = 16$ Ω. Fig. 22(a) shows primary-side voltages $(V_{\rm a1b1}, V_{\rm a2b2})$ and currents $(i_{\rm pri1}, i_{\rm pri2})$ when the module 1 is working and module 2 is shut off. By controlling the MC-CB selector, the module 2 is adding on load. Fig. 22(b) shows primary-side voltages $(V_{\rm a1b1}, V_{\rm a2b2})$ and currents $(i_{\rm pri1}, i_{\rm pri2})$ when the both module 1 and module 2 are working. And the transient waveforms of primary-side voltages $(V_{\rm a1b1}, V_{\rm a2b2})$ and currents $(i_{\rm pri1}, i_{\rm pri2})$ are shown in Fig. 23 when the module 2 is adding and returning

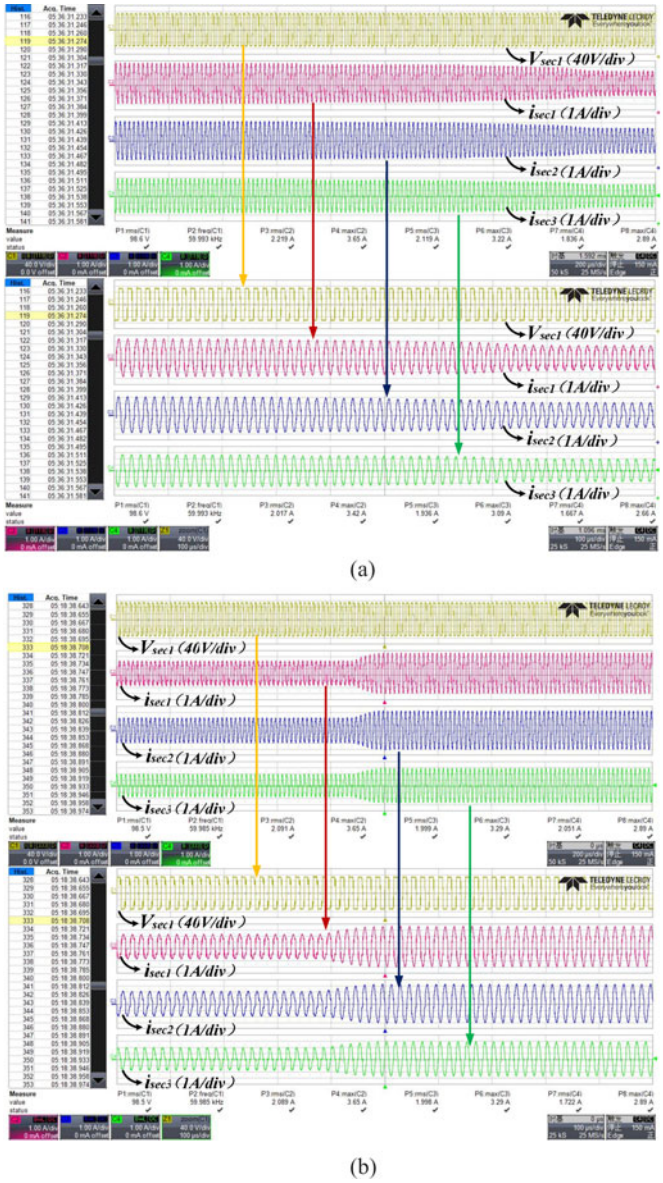

Fig. 20. Transient waveforms of three *LLC* resonant converters: (a) Secondary-side voltage $V_{\rm sec1}$ and currents $(i_{\rm sec1}, i_{\rm sec2}, i_{\rm sec3})$ during a step up of resistive load from $R_0 = 16$ Ω to 27 Ω. (b) Secondary-side voltage $V_{\rm sec1}$ and currents $(i_{\rm sec1}, i_{\rm sec2}, i_{\rm sec3})$ during a step down of resistive load from $R_0 =$ 27 to 16 Ω.

on load. From Fig. 23, we can see the primary-side currents $(i_{\rm pri1}, i_{\rm pri2})$ of the two *LLC* resonant converters get nearly the same within the extremely short time.

So the experiment results prove the MC-CB cells can work well when the modules currents have a big difference initially. And the MC-CB selector can be used for adding and returning modules on load.

In the end, the experimental results indicate that ICS and OCS performance have been achieved well in the proposed MC-CB-cell-based IPOP *LLC* resonant converter modules.

And the steady-state and dynamic-state current-sharing performance of the IPOP converter system are analyzed to verify the good ability of MC-CB cells.

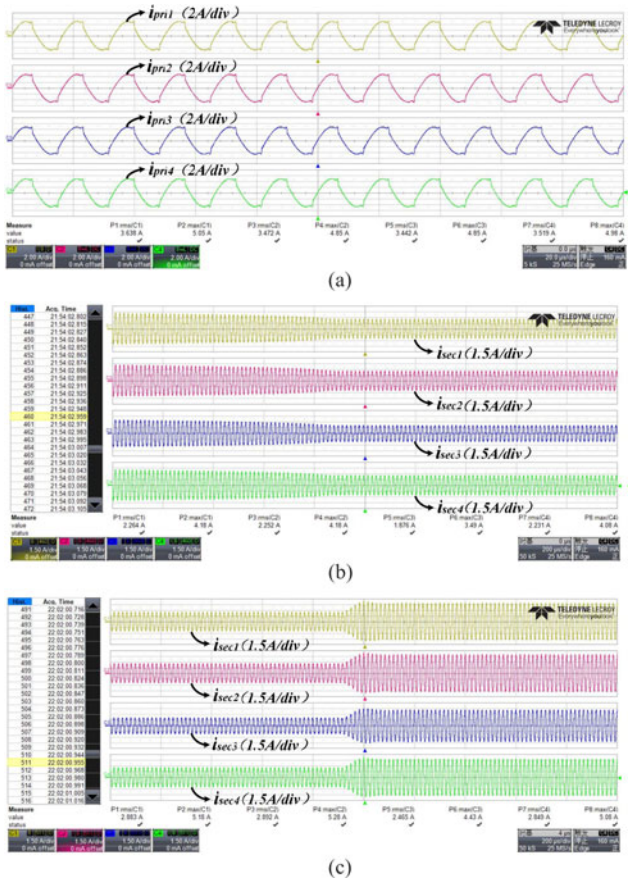

Fig. 21. Steady-state and dynamic-state current-sharing performance of the four-module IPOP converter system: (a) Primary-side currents ($i_{\mathrm{pri1}}, i_{\mathrm{pri2}}, i_{\mathrm{pri3}}, i_{\mathrm{pri4}}$) of four *LLC* resonant converter modules. (b) Secondary-side currents ($i_{\mathrm{sec1}}, i_{\mathrm{sec2}}, i_{\mathrm{sec3}}, i_{\mathrm{sec4}}$) during a step up of resistive load from $R_0 = 8$ to 16 Ω. (c) Secondary-side currents ($i_{\mathrm{sec1}}, i_{\mathrm{sec2}}, i_{\mathrm{sec3}}, i_{\mathrm{sec4}}$) during a step down of resistive load from $R_0 = 16$ to 8 Ω.

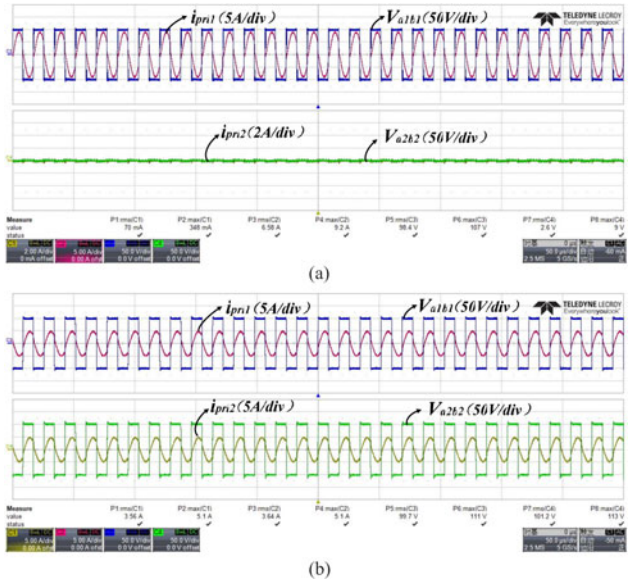

Fig. 22. Experimental results of two-module IPOP system with the MC-CB selector: (a) Primary-side voltages ($V_{\mathrm{a1b1}}, V_{\mathrm{a2b2}}$) and currents ($i_{\mathrm{pri1}}, i_{\mathrm{pri2}}$) when the module 1 is working and module 2 is shut off. (b) Primary-side voltages ($V_{\mathrm{a1b1}}, V_{\mathrm{a2b2}}$) and currents ($i_{\mathrm{pri1}}, i_{\mathrm{pri2}}$) when the both module 1 and module 2 are working.

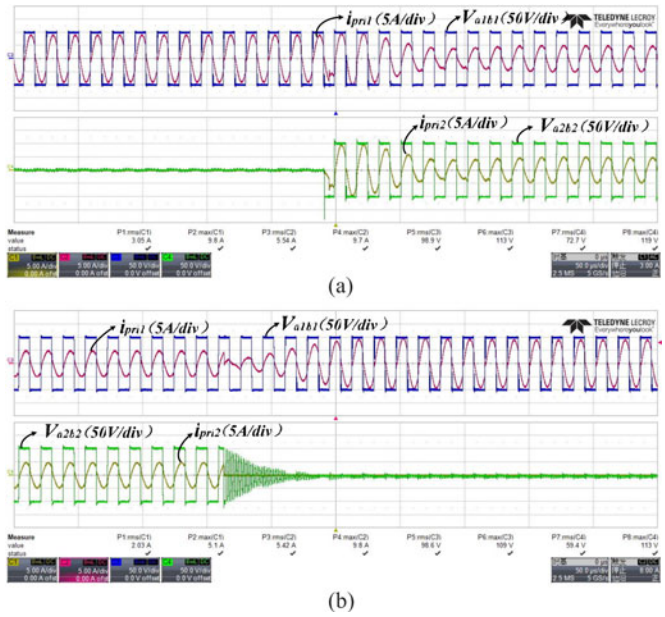

Fig. 23. Transient waveforms of primary-side voltages ($V_{\mathrm{a1b1}}, V_{\mathrm{a2b2}}$) and currents ($i_{\mathrm{pri1}}, i_{\mathrm{pri2}}$) when the module 2 is adding and returning on-load: (a) adding module 2 on load and (b) returning module 2 on load.

V. Conclusion

In this paper, an IPOP *LLC* resonant converter modules based dc–dc system is proposed under the quasi-resonant mode. Unlike the existing closed loop for IPOP system, the MC-CB method is adopted to realize ICS and OCS among all modules with open-loop operating condition naturally. Based on the proposed magnetic model of MC-CB cell, the steady-state and dynamic-state current-sharing performance of the IPOP converter system has been analyzed and the experimental results of the hardware prototype have verified the validity and good performance of the proposed MC-CB cells. Additionally, the method seems to be simple, reliable and easy expansion.

References

[1] J-.H. Jung, H-.S. Kim, M-.H. Ryu, and J-.W. Baek, "Design methodology of bidirectional CLLC resonant converter for high-frequency isolation of DC distribution systems," *IEEE Trans. Power Electron.*, vol. 28, no. 4, pp. 1741–1755, Apr. 2013.

[2] D. Dong, I. Cvetkovic, D. Boroyevich, W. Zhang, R. Wang, and P. Mattavelli, "Grid-interface bidirectional converter for residential DC distribution systems—Part one: High-density two-stage topology," *IEEE Trans. Power Electron.*, vol. 28, no. 4, pp. 1655–1666, Apr. 2013.

[3] T. F. Wu, Y. K. Chen, G. R. Yu, and Y. C. Chang, "Design and development of DC-distributed system with grid connection for residential applications," in *Proc. IEEE Int. Conf. Power Electron. ECCE Asia*, May/Jun. 2011, pp. 235–241.

[4] S. Xu, A. Q. Huang, and R. Burgos, "Review of solid-state transformer technologies and their application in power distribution systems," *IEEE J. Emerg. Sel. Topics Power Electron.*, vol. 1, no. 3, pp. 186–198, Sep. 2013.

[5] C. Y. Gu, Z. D. Zheng, L. Xu, K. Wang, and Y. D. Li, "Modeling and control of a multiport power electronic transformer (PET) for electric traction applications," *IEEE Trans. Power Electron.*, vol. 31, no. 2, pp. 915–927, Feb. 2016.

[6] S. M. Lambert, V. Pickert, D. J. Atkinson, and H. X. Zhan, "Transformer-based equalization circuit applied to N-number of high capacitance cells," *IEEE Trans. Power Electron.*, vol. 31, no. 2, pp. 1334–1343, Feb. 2016.

[7] F. Blaabjerg, A. Consoli, J. A. Ferreira, and J. D. Van Wyk, "The future of electronic power processing and conversion," *IEEE Trans. Power Electron.*, vol. 20, no. 3, pp. 715–720, May 2005.
[8] P. T. Krein, R. S. Balog, and M. Mirjafari, "Minimum energy and capacitance requirements for single-phase inverters and rectifiers using a ripple port," *IEEE Trans. Power Electron.*, vol. 27, no. 11, pp. 4690–4698, Nov. 2012.
[9] W. Pei, W. Deng, X. Zhang, H. Qu, and K. Sheng, "Potential of using multiterminal LVDC to improve plug-in electric vehicle integration in an existing distribution network," *IEEE Trans. Ind. Electron.*, vol. 62, no. 5, pp. 3101–3111, May 2015.
[10] O. Lucia, I. Cvetkovic, H. Sarnago, D. Boroyevich, P. Mattavelli, and F. C. Lee, "Design of home appliances for a DC-based nanogrid system: An induction range study case," *IEEE J. Emerg. Sel. Topics Power Electron.*, vol. 1, no. 4, pp. 315–326, Dec. 2013.
[11] J. Rodriguez, J-.S. Lai, and F. Z. Peng, "Multilevel inverters: A survey of topologies, controls, and applications," *IEEE Trans. Ind. Electron.*, vol. 49, no. 4, pp. 724–738, Aug. 2002.
[12] C. Liu, P. W. Sun, J-.S. Lai, Y. C. Ji, M. Y. Wang, C.-L. Chen, and G. W. Cai, "Cascade dual-boost/buck active-front-end converter for intelligent universal transformer," *IEEE Trans. Ind. Electron.*, vol. 59, no. 12, pp. 4671–4680, Dec. 2012.
[13] B. Gultekin and M. Ermis, "Cascaded multilevel converter-based transmission STATCOM: System design methodology and development of a 12 kV $\pm$12 MVAr power stage," *IEEE Trans. Power Electron.*, vol. 28, no. 11, pp. 4930–4950, Nov. 2013.
[14] P. Sotoodeh and R. D. Miller, "Design and Implementation of an 11-level inverter with FACTS capability for distributed energy systems," *IEEE J. Emerging Sel. Topics Power Electron.*, vol. 2, no. 1, pp. 87–96, Mar. 2014.
[15] M. Pahlevani, S. Eren, A. Bakhshai, and P. Jain, "A series–parallel current-driven full-bridge DC/DC converter," *IEEE Trans. Power Electron.*, vol. 31, no. 2, pp. 1275–1293, Feb. 2016.
[16] H. Renaudineau, J. -P. Martin, B. Nahid-Mobarakeh, and S. Pierfederici, "DC–DC converters dynamic modeling with state observer-based parameter estimation," *IEEE Trans. Power Electron.*, vol. 30, no. 6, pp. 3356–3363, Jun. 2015.
[17] X. Wu, X. Xie, J. Zhang, R. Zhao, and Z. Qian, "Soft switched full bridge DC–DC converter with reduced circulating loss and filter requirement," *IEEE Trans. Power Electron.*, vol. 22, no. 5, pp. 1949–1955, Sep. 2007.
[18] C. Liu, A. Johnson, and J. S. Lai, "A novel three-phase high-power soft-switched DC/DC converter for low-voltage fuel cell applications," *IEEE Trans. Power Electron.*, vol. 41, no. 6, pp. 1691–1697, Nov./Dec. 2005.
[19] Y. C. Ren, M. Xu, J. Sun, and F. C. Lee, "A family of high power density unregulated bus converters," *IEEE Trans. Power Electron.*, vol. 20, no. 5, pp. 1045–1054, Sep. 2005.
[20] N. Shafiei and M. Ordonez, "Improving the regulation range of EV battery chargers with L3C2 resonant converters," *IEEE Trans. Power Electron.*, vol. 30, no. 6, pp. 3166–3184, Jun. 2015.
[21] M. Z. Youssef and P. K. Jain, "Series-parallel resonant converter in self-sustained oscillation mode with the high-frequency transformer-leakage-inductance effect: Analysis, modeling, and design," *IEEE Trans. Ind. Electron.*, vol. 54, no. 3, pp. 1329–1341, Jun. 2007.
[22] J.-Y. Shin, H.-W. Kim, K.-Y. Cho, S.-S. Hwang, S.-K. Chung, and G.-B. Chung, "Analysis of *LLC* resonant converter with current-doubler rectification circuit," in *Proc. 2014 16th Int. Power Electron. Motion Control Conf. Expo.*, Sep. 21–24, pp. 162–167.
[23] H. Hu, X. Fang, F. Chen, Z. J. Shen, and I. Batarseh, "A modified high-efficiency LLC converter with two transformers for wide input-voltage range applications," *IEEE Trans. Power Electron.*, vol. 28, no. 4, pp. 1946–1960, Apr. 2013.
[24] C. Adragna, S. D. Simone, and C. Spini, "Designing LLC resonant converters for optimum efficiency," in *Proc. Eur. Conf. Power Electron. Appl.*, Sep. 2009, pp. 1–10.
[25] X. G. Xie, J. M. Zhang, C. Zhao, Z. Zhao, and Z. M. Qian, "Analysis and optimization of LLC resonant converter with a novel over-current protection circuit," *IEEE Trans. Power Electron.*, vol. 22, no. 2, pp. 435–443, Mar. 2007.
[26] R. Beiranvand, B. Rashidian, M. R. Zolghadri, and S. M. H. Alavi, "Using LLC resonant converter for designing wide-range voltage source," *IEEE Trans. Ind. Electron.*, vol. 58, no. 5, pp. 1746–1756, May 2011.
[27] Z. Y. Hu, Y. J. Qiu, L. L. Wang, and Y. F. Liu, "An interleaved LLC resonant converter operating at constant switching frequency," *IEEE Trans. Power Electron.*, vol. 29, no. 6, pp. 2931–2943, Jun. 2014.
[28] W. Chen, P. Rong, and Z. Y. Lu, "Snubberless bidirectional DC–DC converter with new CLLC resonant tank featuring minimized switching loss," *IEEE Trans. Ind. Electron.*, vol. 57, no. 9, pp. 3075–3086, Sep. 2010.
[29] T. Y. Jiang, J. M. Zhang, X. K. Wu, K. Sheng, and Y. S. Wang, "A bidirectional LLC resonant converter with automatic forward and backward mode transition," *IEEE Trans. Power Electron.*, vol. 30, no. 2, pp. 757–770, Feb. 2015.
[30] J. J. Shi, T. J. Liu, J, Cheng, and X. N. He, "Automatic current sharing of an input-parallel output-parallel (IPOP)-connected DC–DC converter system with chain-connected rectifiers," *IEEE Trans. Power Electron.*, vol. 30, no. 6, pp. 2997–3016, Jun. 2015.
[31] D. S. Sha, Z. Q. Guo, and X. Z. Liao, "Control strategy for input-parallel–output-parallel connected high-frequency isolated inverter modules," *IEEE Trans. Power Electron.*, vol. 26, no. 8, pp. 2237–2248, Aug. 2011.
[32] J. Shi, L. Zhou, and X. He, "Common-duty-ratio control of input-parallel output-parallel (IPOP) connected DC–DC converter modules with automatic sharing of currents," *IEEE Trans. Power Electron.*, vol. 27, no. 7, pp. 3277–3291, Jul. 2012.
[33] J. Cheng, J. J. Shi, and X. N. He, "A novel input-parallel output-parallel connected DC-DC converter module with automatic sharing of currents," in *Proc. 2012 7th Int. Power Electron. Motion Control Conf.*, Jun. 2–5, vol. 3, pp. 1871–1876.
[34] F. Wang, Y. Wang, Q. Gao, C. M. Wang, and Y. B. Liu, "A control strategy for suppressing circulating currents in parallel-connected PMSM drives with individual DC links," *IEEE Trans. Power Electron.*, vol. 31, no. 2, pp. 1680–1691, Feb. 2016.
[35] Y. Yu, G. Konstantinou, B. Hredzak, and V. G. Agelidis, "Power balance optimization of cascaded h-bridge multilevel converters for large-scale photovoltaic integration," *IEEE Trans. Power Electron.*, vol. 31, no. 2, pp. 1108–1120, Feb. 2016.
[36] S. Zong, H. Z. Luo, W. H. Li, X. N. He, and C. L. Xia, "Theoretical evaluation of stability improvement brought by resonant current loop for paralleled LLC converters," *IEEE Trans. Ind. Electron.*, vol. 62, no. 7, pp. 4170–4180, Jul. 2015.

Chuang Liu received the M.S. degree in electrical engineering from Northeast Dianli University, Jilan, China, in 2009, and the Ph.D. degree from Harbin Institute of Technology, Harbin, China, in 2013.

From 2010 to 2012, he was with Future Energy Electronics Center (FEEC), Virginia Tech, Blacksburg, USA, as a Visiting Ph.D. Student, supported by the Chinese Scholarship Council. Since 2013, he has been an Associate Professor at the School of Electrical Engineering, Northeast Dianli university. His current research interests include solid-state substation based on power electronics transformer for future hybrid ac/dc power grid, PHEV/PEV smart parking lot/building charging system, battery energy storage systems, and wireless power transfer.

Xinzhe Xu received the B.S. degree from North China Electric Power University, Beijing, China, in 2013. He is currently working toward the M.S. degree in the Department of Electrical Engineering, Northeast Dianli University, Jilin, China.

He is also with Beijing Electric Power Corporation, State Grid Corporation of China, Beijing. His current research interests include intelligent universal transformers (IUT) for renewable energy systems.

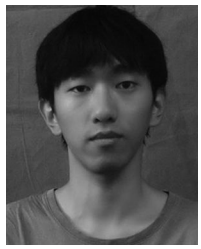

Dacheng He received the B.S. degree in 2014 from Northeast Dianli University, Jilin, China, where she is currently working toward the M.S. degree in the Electrical Engineering Department.

His current research interests include electric motor drives and power electronics.

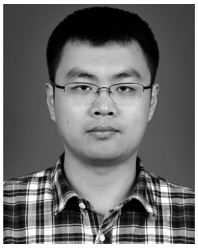

Haiyang Liu received the B.S. degree from the Huazhong University of Science and Technology, Wuhan, China, in 2012. He is currently working toward the M.S. degree in the Department of Electrical Engineering, Northeast Dianli University, Jilin, China.

His current research interests include intelligent universal transformers (IUT) for renewable energy systems.

Xiaotong Tian received the B.S. degree in 2014 from Northeast Dianli University, Jilin, China where she is currently working toward the M.S. degree in the Electrical Engineering Department.

His current research interests include electric motor drives and power electronics.

Ying Guo received the B.S. degree from the Qingdao Technological University, Qingdao, China, in 2012. He is currently working toward the M.S. degree in the Department of Electrical Engineering, Northeast Dianli University, Jilin, China.

His current research interest includes wireless power transfer (WPT).

Guowei Cai received the B.S. and M.S. degrees from Northeast Dianli University, Jilin, China, in 1990 and 1993, respectively, and the Ph.D. degree from Harbin Institute of Technology, Harbin, China, in 1999.

Since 2004, he has been a Professor at the School of Electrical Engineering, Northeast Dianli University. His current research interests include power system transient stability analysis and electrical power markets.

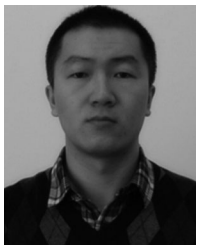

Chenglian Ma received the M.S. degree in electrical engineering from Northeast Dianli University, Jilin, China, in 2009. He is currently working toward the Ph.D. degree from the School of Electrical and Electronic Engineering, North China Electric Power University, Beijing, China.

His current research interests include power system safety operation and control, HVDC connected issues related to the ends of the earth, and other aspects.

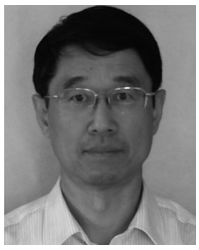

Gang Mu received the B.S. and M.S. degrees from Northeast Dianli University, Jilin, China, in 1981 and 1984, respectively, and the Ph.D. degree from Tsinghua University, Beijing, China, in 1991.

Since 1994, he has been a Professor at the School of Electrical Engineering, Northeast Dianli University. His current research interests include key technologies of large-scale incorporated operation analysis, transient stability analysis, and control power system.